

Operator Autoencoders: Learning Physical Operations on Encoded Molecular Graphs

Willis Hoke¹, Daniel Shea², and Stephen Casey³

Abstract—Molecular dynamics simulations produce data with complex nonlinear dynamics. If the timestep behavior of such a dynamic system can be represented by a linear operator, future states can be inferred directly without expensive simulations. The use of an autoencoder in combination with a physical timestep operator allows both the relevant structural characteristics of the molecular graphs and the underlying physics of the system to be isolated during the training process. In this work, we develop a pipeline for establishing graph-structured representations of time-series volumetric data from molecular dynamics simulations. We then train an autoencoder to find nonlinear mappings to a latent space where future timesteps can be predicted through application of a linear operator trained in tandem with the autoencoder. Increasing the dimensionality of the autoencoder output is shown to improve the accuracy of the physical timestep operator.

I. INTRODUCTION

RESEARCH into generating graph structures with desired properties has a history dating at least as far back as 1960 [1], with several diverse approaches having subsequently been developed related to statistical graph representation [2]-[5]. Prior work developing generative models for molecular structures [6] has demonstrated the usefulness of graph representations for volumetric data. Concurrently, deep learning techniques have demonstrated notable success in various domains including imaging [7],[8], text [9],[10], and speech [11],[12]. Graph-related deep learning methods have been developed in recent years, focusing on areas such as graph generators [13], graph representation learning methods [14]-[18], graph attention models [19], and attack and defense techniques on graph data [20].

Graph autoencoders are neural networks trained to represent the structural features of a set of graph adjacency matrices as a vector of latent space variables [21]-[38]. Neural networks provide a powerful tool for nonlinear dimensionality transformation; in cases where input data do not lie on a linear manifold, an autoencoder can learn a mapping to a higher- or lower-dimensional space capturing the inherent structure of the data. However, autoencoded adjacency matrices can become computationally intractable for graphs with large numbers of nodes [6]. To overcome this limitation for large molecular graphs we find the local graph representation in the neighborhood around each atom, thereby creat-

ing a set of overlapping subgraphs in 3D space. Each subgraph is encoded into a corresponding latent vector.

Graph decoding is the inverse of the encoding function whereby the latent vectors are reconstituted into adjacency matrices. These adjacency matrices produce overlapping subgraphs which must undergo a graph-matching procedure in order to reconstruct the full volume. Studies in graph matching have considered this problem from deep learning and combinatorial optimization perspectives [39]-[42]. To assist with reconstruction of our full-volume molecular graph, we introduce a canonical graph representation which eliminates the need for computationally expensive graph matching methods otherwise required to determine the similarity of overlapping graphs.

In addition to autoencoding, recent works have used deep neural networks to discover advantageous coordinate transformations for dynamic systems [43]-[50]. Such a transformation function can be modelled as linear Koopman operator acting on a state space of system observables [51]-[55]. Following results shown by [56], we train an autoencoder in parallel with a linear operator and demonstrate the use of high-dimensional latent representations to facilitate discovery of linear models for local system dynamics. Our model is trained on time-series data of diamond structures subjected to tensile deformation in the LAMMPS molecular dynamics simulation environment.

II. METHODS

A. Subvolume Sampling

To learn approximations of global system dynamics, we consider local neighborhoods of atoms within a larger molecular structure. This has the dual advantage of shortening computation time caused by encoding large graphs while improving results in cases where local system dynamics are better approximated by a linear operator than global dynamics. By oversampling subsets of the initial dataset, we ensure graph representations of subvolumes can be projected back into three-dimensional coordinate space aligned to reconstruct the original volume.

Initial experiments utilized cubical subvolumes sampled along a grid. However, even in the optimal case this gives subvolumes of different sizes, which required zero-padding distance matrices after finding graph representations. Thus, a k -nearest neighbors algorithm was applied to each point in the initial volume to generate n subvolumes with k points each.

Since the LAMMPS [57] environment can use pe-

¹Department of Computer Science, Portland State University

²Department of Materials Science and Engineering, University of Washington

³NASA Langley Research Center; e-mail: Stephen.Casey@nasa.gov

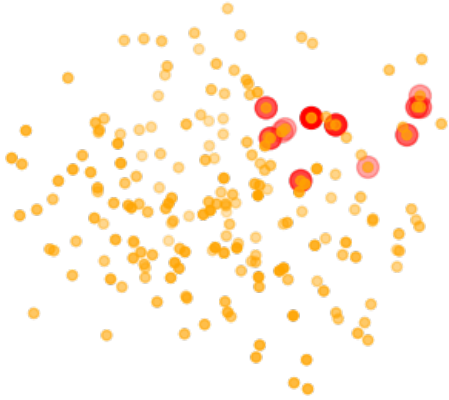


Fig. 1: Example subvolume (red) found using K -Nearest Neighbors

riodic boundary conditions for molecular dynamics simulations, we truncate the initial volumetric data to exclude atoms within a certain percent p distance from the bounding box. We found $p = 5$ to be a sufficient value to eliminate boundary artifacts. This prevents sudden variations in atomic position between consecutive time steps.

B. Distance Matrices & Bond Order Potentials

Graph representations have clear advantages over coordinate representations for learning latent embeddings. First, since they explicitly represent the relationships between atoms in a subvolume, they directly capture structural features. Secondly, since graph representations are invariant to linear or affine transformation, they provide a compact representation for volumes with similar structural features.

Pairwise distances are calculated between atoms in each subvolume using a standard Euclidean metric to yield the matrix $D \in \mathbb{R}^{k \times k}$. Reconstruction from distance matrices was demonstrated on randomized data using classical Multi-Dimensional Scaling (MDS) followed by Procrustes reconstruction.

Bond order potentials are next calculated from the pairwise distance matrix. We chose a two-body potential as three-body potentials require a significant number of parameters, some of which are unknown or unverified. The Lennard Jones potential is calculated as

$$V_{LJ}(r) = 4\varepsilon \left[\left(\frac{\sigma}{r} \right)^{12} - \left(\frac{\sigma}{r} \right)^6 \right] \quad (1)$$

Here ε and σ are parameters chosen specifically according to atom types and molecular configuration. We used $\varepsilon = 0.7$ and $\sigma = 1.45$ based on experimental parameters for similar carbon structures [58].

C. Canonical Graph Representations

Past examples of graph autoencoders [6] have relied on approximation strategies like Max Pooling Matching (MPM)[59] to evaluate graph similarity. Since evaluation is computationally expensive and occurs in the loss function, training becomes intractable for larger molecule sizes. Our alternative approach involves preprocessing all graphs such that

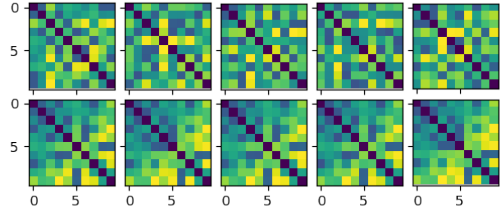


Fig. 2: Similar distance matrices (top) with corresponding canonical representations (bottom)

any permutation of the indices of the adjacency matrix maps to the same representation. We define the ordering mapping a graph to its canonical representation by ordering the indices of a distance matrix according to their magnitude:

$$\mathbf{p} = [i_1 \ i_2 \ \dots \ i_n] : \quad (2)$$

$$\|D_{(i_k)}\| < \|D_{(i_{k+1})}\| \ \forall k \in \{1, 2, \dots, n-1\}$$

The vector \mathbf{p} uniquely determines the permutation applied to the rows and columns of a distance matrix. Not only does the canonical ordering map different representations of the same graph to the same representation, it also yields similar orderings for similar graphs. We tested this hypothesis by generating random permutations of the same distance matrix, adding a small amount of Gaussian noise, then computing canonical representations. As can be seen in Figure 2, the canonical representation is invariant to permutation and resilient to small perturbations of pairwise distances, with the large majority of rows and columns remaining in the same canonical order.

D. Dataset

Our dataset was generated from a simulation of a diamond structure containing 1,000 carbon atoms subjected to tensile deformation over a total of 10 time steps sampled at intervals of 1,000. We selected $k = 10$ to generate subvolumes with 10 atoms each. Pairwise distances were computed using the standard Euclidean metric, then bond-order potentials were computed using the formula outlined above. Data were then separated into pairs of vectors containing upper triangular entries from bond-order potential matrices at consecutive time steps. Finally, data was scaled to the range $[0, 1]$ using a standard min-max scaling algorithm. The final training dataset contained 5,248 pairs of input vectors $v_{t_i}, v_{t_{i+1}} \in \mathbb{R}^{\frac{k(k-1)}{2}}$. A separate test dataset is not utilized since the goal is to learn a linear representation of system dynamics rather than generalizing to unseen data.

E. Model Architecture

The operator-autoencoder model consists of two networks trained in parallel. The first network is a multi-layer autoencoder, while the second represents a weight matrix defining a linear operator.

For the autoencoder, we chose a network with a total of four fully connected feed-forward layers, with the encoder and decoder each containing two layers. Hidden dimension h for hidden layers in encoder and decoder was rounded to the nearest integer to the mean of the input and latent dimensions. Rectified Linear Units (ReLU) were used as activation functions between all layers except the final layer in the decoder, where we used a sigmoidal activation function to constrain output to the range $[0, 1]$.

The linear operator consists of a matrix $M \in \mathbb{R}^{d \times d}$, where d is the dimension of the latent space. The initial value of the operator is set to the identity matrix I_m as this preserves the initial representation of a subvolume and provides the closest known approximation to the next time step.

F. Loss Functions

We utilize two separate loss functions for model training. The first loss function quantifies reconstruction error from the autoencoder using Mean Squared Error (MSE) between an initial subvolume and its reconstruction. Reconstruction loss is defined as:

$$\mathcal{L}_{\mathcal{AE}} = \|\hat{u}_j^{(t_i)} - u_j^{(t_i)}\|_2^2 \quad (3)$$

The second loss function provides a metric for accuracy of the time step operator. Operator loss is defined using MSE between the predicted and actual latent representation at time step $t + 1$:

$$\mathcal{L}_{\mathcal{OP}} = \alpha \|M(v_j^{(t_i)}) - v_j^{(t_{i+1})}\|_2^2 \quad (4)$$

Here α is a hyperparameter which determines the relative contribution of operator loss. Since operator loss backpropagates through the encoder, setting too small a value for α can result in the operator loss steadily increasing over time as the reconstruction loss dominates.

G. Training

During each training epoch, mini-batches consisting of training data representing pairs $(u^{(t_i)}, u^{(t_{i+1})})$ of subvolumes at consecutive time steps pass through the autoencoder to yield latent representations $(v^{(t_i)}, v^{(t_{i+1})})$ and reconstructions $(\hat{u}^{(t_i)}, \hat{u}^{(t_{i+1})})$. The operator M is applied to find $M(v^{(t_i)})$ during the forward pass. Reconstruction and operator loss are computed, then weights for the autoencoder network and operator matrix are updated through backpropagation. This affects the weights of both the operator and the encoder.

After hand-tuning hyperparameters to minimize loss values, we settled on a learning rate of 0.001 with operator training delay of 50 epochs. We fixed the operator loss coefficient $\alpha = 20$. The ADAM optimizer was used for training with a batch size of 64. We trained a total of 9 models for 1500 epochs each. In contrast to typical autoencoder architectures which utilize a low-dimensional latent representation, we instead experiment with various dimension sizes ranging from small to large. For the

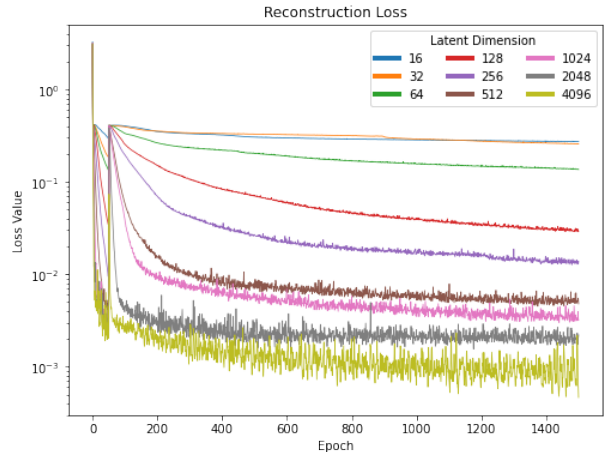


Fig. 3: Reconstruction loss as a function of latent dimension

purpose of training a linear operator, we find larger latent spaces can yield representations with lower operator loss.

III. RESULTS

d	$\min(\mathcal{L}_{\mathcal{AE}})$	$\min(\mathcal{L}_{\mathcal{OP}})$
16	0.2724	0.0013
32	0.1831	0.0026
64	0.1315	0.0058
128	0.0288	0.0040
256	0.0086	0.0024
512	0.0041	0.0012
1024	0.0030	0.0008
2048	0.0016	0.0005
4096	0.0005	0.0003

Minimum loss values as a function of latent dimension

Figure 3 shows results for α -scaled reconstruction loss for each model. In every case the introduction of the operator loss $\mathcal{L}_{\mathcal{OP}}$ after a delay of 50 epochs causes reconstruction loss $\mathcal{L}_{\mathcal{AE}}$ to spike sharply. For lower-dimensional latent representations, reconstruction loss never recovers from this initial dip. However, with higher-dimensional representations, the loss begins to steadily decrease before approaching a steady state. In the case of $d = 4096$, loss values lower than those prior to introduction of the operator loss function can be observed.

Figure 4 shows results for operator loss. As opposed to reconstruction loss, we can observe operator loss rising significantly as the autoencoder network weights are updated during the first 50 training epochs. When operator loss is introduced, loss quickly drops before plateauing. Lower-dimensional latent representations show some variation in the loss surface. This is a result of the two loss functions both affecting the encoder weights. As the encoder learns latent representations with low reconstruction error, it also simultaneously find representations with a high degree of linearity.

Our results demonstrate a strong inverse correlation between latent dimensionality and loss values. High-dimensional latent representations result

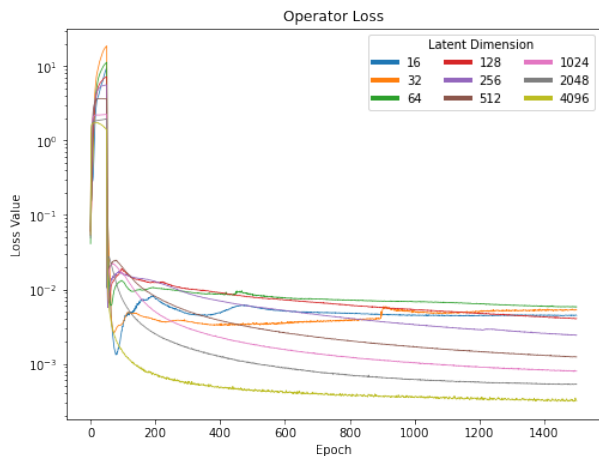


Fig. 4: Operator loss as a function of latent dimension

in models which outperform their low-dimensional analogs by several orders of magnitude. In all cases, minimum operator loss after training is at least a single order of magnitude lower than initial operator loss. However, introduction of the operator loss function significantly limits the performance of the autoencoder when latent dimensionality is low.

IV. CONCLUSION

This work demonstrates the application of a series of invertible transformations to time-series volumetric data to allow an autoencoder to learn efficient latent representations. Graph canonization is shown to be an efficient alternative to graph similarity metrics like MPM during the process of volumetric graph reconstruction. We conclude from our results that high-dimensional latent representations display strong linearity and show lowest values for both autoencoder and timestep operator loss metrics. Learned linear timestep operators show minimal loss when applied to vectors in the latent space.

Natural extensions to this work could involve assessing the effects of repeated applications of the linear timestep operator, removing linearity constraints on the timestep operator, testing with other types of materials, and testing with other types of physical processes in addition to mechanical deformation. The model can also be extended to high-dimensional data; while the architecture was developed with molecular data in mind, it should be possible to find a mapping to a representative latent space for any arbitrary set of time-series data.

REFERENCES

- [1] Paul Erdős and Alfréd Rényi, "On the evolution of random graphs," *Publ. Math. Inst. Hung. Acad. Sci.*, vol. 5, no. 1, pp. 17–60, 1960.
- [2] Duncan J Watts and Steven H Strogatz, "Collective dynamics of 'small-world' networks," *nature*, vol. 393, no. 6684, pp. 440–442, 1998.
- [3] Réka Albert and Albert-László Barabási, "Statistical mechanics of complex networks," *Reviews of modern physics*, vol. 74, no. 1, pp. 47, 2002.
- [4] Paul W Holland, Kathryn Blackmond Laskey, and Samuel Leinhardt, "Stochastic blockmodels: First steps," *Social networks*, vol. 5, no. 2, pp. 109–137, 1983.
- [5] Jure Leskovec, Deepayan Chakrabarti, Jon Kleinberg, Christos Faloutsos, and Zoubin Ghahramani, "Kronecker

- graphs: an approach to modeling networks.," *Journal of Machine Learning Research*, vol. 11, no. 2, 2010.
- [6] Martin Simonovsky and Nikos Komodakis, "Graphvae: Towards generation of small graphs using variational autoencoders," in *International Conference on Artificial Neural Networks*. Springer, 2018, pp. 412–422.
- [7] Yang Yu, Zhiqiang Gong, Ping Zhong, and Jiaxin Shan, "Unsupervised representation learning with deep convolutional neural network for remote sensing images," in *International Conference on Image and Graphics*. Springer, 2017, pp. 97–108.
- [8] Xinchun Yan, Jimei Yang, Kihyuk Sohn, and Honglak Lee, "Attribute2image: Conditional image generation from visual attributes," in *European Conference on Computer Vision*. Springer, 2016, pp. 776–791.
- [9] Yizhe Zhang, Zhe Gan, Kai Fan, Zhi Chen, Ricardo Henao, Dinghan Shen, and Lawrence Carin, "Adversarial feature matching for text generation," in *International Conference on Machine Learning*. PMLR, 2017, pp. 4006–4015.
- [10] Prince Zizhuang Wang and William Yang Wang, "Riemannian normalizing flow on variational wasserstein autoencoder for text modeling," *Proceedings of the 2019 Conference of the North American Chapter of the Association for Computational Linguistics: Human Language Technologies*, pp. 284–294, 2019.
- [11] Takuhiro Kaneko, Hirokazu Kameoka, Kaoru Hiramatsu, and Kunio Kashino, "Sequence-to-sequence voice conversion with similarity metric learned using generative adversarial networks.," in *INTERSPEECH*, 2017, vol. 2017, pp. 1283–1287.
- [12] Yang Gao, Rita Singh, and Bhiksha Raj, "Voice impersonation using generative adversarial networks," in *2018 IEEE International Conference on Acoustics, Speech and Signal Processing (ICASSP)*. IEEE, 2018, pp. 2506–2510.
- [13] Faezeh Faez, Yassaman Ommi, Mahdiah Soleymani Baghshah, and Hamid R Rabiee, "Deep graph generators: A survey," *arXiv preprint arXiv:2012.15544*, 2020.
- [14] Ziwei Zhang, Peng Cui, and Wenwu Zhu, "Deep learning on graphs: A survey," *IEEE Transactions on Knowledge and Data Engineering*, 2020.
- [15] Zonghan Wu, Shirui Pan, Fengwen Chen, Guodong Long, Chengqi Zhang, and S Yu Philip, "A comprehensive survey on graph neural networks," *IEEE transactions on neural networks and learning systems*, 2020.
- [16] Jie Zhou, Ganqu Cui, Shengding Hu, Zhengyan Zhang, Cheng Yang, Zhiyuan Liu, Lifeng Wang, Changcheng Li, and Maosong Sun, "Graph neural networks: A review of methods and applications," *AI Open*, vol. 1, pp. 57–81, 2020.
- [17] Wenming Cao, Zhiyue Yan, Zhiquan He, and Zhihai He, "A comprehensive survey on geometric deep learning," *IEEE Access*, vol. 8, pp. 35929–35949, 2020.
- [18] Davide Bacciu, Federico Errica, Alessio Micheli, and Marco Podda, "A gentle introduction to deep learning for graphs," *Neural Networks*, 2020.
- [19] John Boaz Lee, Ryan A Rossi, Sungchul Kim, Nesreen K Ahmed, and Eunyee Koh, "Attention models in graphs: A survey," *ACM Transactions on Knowledge Discovery from Data (TKDD)*, vol. 13, no. 6, pp. 1–25, 2019.
- [20] Lichao Sun, Yingtong Dou, Carl Yang, Ji Wang, Philip S Yu, Lifang He, and Bo Li, "Adversarial attack and defense on graph data: A survey," *arXiv preprint arXiv:1812.10528*, 2018.
- [21] Wengong Jin, Regina Barzilay, and Tommi Jaakkola, "Hierarchical generation of molecular graphs using structural motifs," *International Conference on Machine Learning*, 02 2020.
- [22] John Bradshaw, Brooks Paige, Matt J Kusner, Marwin HS Segler, and José Miguel Hernández-Lobato, "A model to search for synthesizable molecules," *Advances in Neural Information Processing Systems*, pp. 7935–7947, 2019.
- [23] Qi Liu, Miltiadis Allamanis, Marc Brockschmidt, and Alexander L Gaunt, "Constrained graph variational autoencoders for molecule design," *Advances in Neural Information Processing Systems*, pp. 7795–7804, 2018.
- [24] Rim Assouel, Mohamed Ahmed, Marwin H Segler, Amir Saffari, and Yoshua Bengio, "Defactor: Differentiable edge factorization-based probabilistic graph generation," *arXiv preprint arXiv:1811.09766*, 2018.
- [25] Shih-Yang Su, Hossein Hajimirsadeghi, and Greg Mori, "Graph generation with variational recurrent neural net-

- work,” *NeurIPS Workshop on Graph Representation Learning*, 2019.
- [26] Jaechang Lim, Sang-Yeon Hwang, Seokhyun Moon, Seungsu Kim, and Woo Youn Kim, “Scaffold-based molecular design with a graph generative model,” *Chemical Science*, vol. 11, no. 4, pp. 1153–1164, 2020.
 - [27] Thomas N Kipf and Max Welling, “Variational graph auto-encoders,” *NeurIPS Workshop on Bayesian Deep Learning*, 2016.
 - [28] Daniel Flam-Shepherd, Tony Wu, and Alan Aspuru-Guzik, “Graph deconvolutional generation,” *arXiv preprint arXiv:2002.07087*, 2020.
 - [29] Tengfei Ma, Jie Chen, and Cao Xiao, “Constrained generation of semantically valid graphs via regularizing variational autoencoders,” *Advances in Neural Information Processing Systems*, pp. 7113â€–7124, 2018.
 - [30] Aditya Grover, Aaron Zweig, and Stefano Ermon, “Graphite: Iterative generative modeling of graphs,” in *International conference on machine learning*. PMLR, 2019, pp. 2434–2444.
 - [31] Xiaojie Guo, Liang Zhao, Zhao Qin, Lingfei Wu, Amarda Shehu, and Yanfang Ye, “Node-edge co-disentangled representation learning for attributed graph generation,” in *International Conference on Knowledge Discovery and Data Mining (SIGKDD)*, 2020.
 - [32] Jia Li, Tomasyu Yu Jiajin Li, Honglei Zhang, Kangfei Zhao, Yu Rong, and Hong Cheng, “Dirichlet graph variational autoencoder,” *Advances in Neural Information Processing Systems*, 2020.
 - [33] Wengong Jin, Regina Barzilay, and Tommi Jaakkola, “Junction tree variational autoencoder for molecular graph generation,” in *International Conference on Machine Learning*. PMLR, 2018, pp. 2323–2332.
 - [34] Hiroshi Kajino, “Molecular hypergraph grammar with its application to molecular optimization,” in *International Conference on Machine Learning*. PMLR, 2019, pp. 3183–3191.
 - [35] Bidisha Samanta, Abir De, Gourhari Jana, Vicenç Gómez, Pratim Kumar Chattaraj, Niloy Ganguly, and Manuel Gomez-Rodriguez, “Nevae: A deep generative model for molecular graphs,” *Journal of machine learning research*. 2020 Apr; 21 (114): 1-33, 2020.
 - [36] Jenny Liu, Aviral Kumar, Jimmy Ba, Jamie Kiros, and Kevin Swersky, “Graph normalizing flows,” *Advances in Neural Information Processing Systems*, pp. 13578â€–13588, 2019.
 - [37] Carl Yang, Peiye Zhuang, Wenhan Shi, Alan Luu, and Pan Li, “Conditional structure generation through graph variational generative adversarial nets,” in *NeurIPS*, 2019, pp. 1338–1349.
 - [38] Wengong Jin, Kevin Yang, Regina Barzilay, and Tommi Jaakkola, “Learning multimodal graph-to-graph translation for molecular optimization,” *International Conference on Learning Representations*, 2018.
 - [39] Yujia Li, Chenjie Gu, Thomas Dullien, Oriol Vinyals, and Pushmeet Kohli, “Graph matching networks for learning the similarity of graph structured objects,” in *International Conference on Machine Learning*. PMLR, 2019, pp. 3835–3845.
 - [40] Matthias Fey, Jan E Lenssen, Christopher Morris, Jonathan Masci, and Nils M Kriege, “Deep graph matching consensus,” *International Conference on Learning Representations*, 2020.
 - [41] Guixiang Ma, Nesreen K Ahmed, Theodore L Willke, and S Yu Philip, “Deep graph similarity learning: A survey,” *Data Mining and Knowledge Discovery*, pp. 1–38, 2021.
 - [42] Junchi Yan, Shuang Yang, and Edwin R Hancock, “Learning for graph matching and related combinatorial optimization problems,” in *International Joint Conference on Artificial Intelligence*. York, 2020.
 - [43] Bethany Lusch, J Nathan Kutz, and Steven L Brunton, “Deep learning for universal linear embeddings of nonlinear dynamics,” *Nature communications*, vol. 9, no. 1, pp. 1–10, 2018.
 - [44] Christoph Wehmeyer and Frank Noé, “Time-lagged autoencoders: Deep learning of slow collective variables for molecular kinetics,” *The Journal of chemical physics*, vol. 148, no. 24, pp. 241703, 2018.
 - [45] Andreas Mardt, Luca Pasquali, Hao Wu, and Frank Noé, “Author correction: Vampnets for deep learning of molecular kinetics,” *Nature communications*, vol. 9, no. 1, pp. 1–1, 2018.
 - [46] Naoya Takeishi, Yoshinobu Kawahara, and Takehisa Yairi, “Learning koopman invariant subspaces for dynamic mode decomposition,” *arXiv preprint arXiv:1710.04340*, 2017.
 - [47] Enoch Yeung, Soumya Kundu, and Nathan Hodas, “Learning deep neural network representations for koopman operators of nonlinear dynamical systems,” in *2019 American Control Conference (ACC)*. IEEE, 2019, pp. 4832–4839.
 - [48] Samuel E Otto and Clarence W Rowley, “Linearly recurrent autoencoder networks for learning dynamics,” *SIAM Journal on Applied Dynamical Systems*, vol. 18, no. 1, pp. 558–593, 2019.
 - [49] Qianxiao Li, Felix Dietrich, Erik M Bollt, and Ioannis G Kevrekidis, “Extended dynamic mode decomposition with dictionary learning: A data-driven adaptive spectral decomposition of the koopman operator,” *Chaos: An Interdisciplinary Journal of Nonlinear Science*, vol. 27, no. 10, pp. 103111, 2017.
 - [50] Craig Gin, Bethany Lusch, Steven L Brunton, and J Nathan Kutz, “Deep learning models for global coordinate transformations that linearize pdes,” *arXiv preprint arXiv:1911.02710*, 2019.
 - [51] Bernard O Koopman, “Hamiltonian systems and transformation in hilbert space,” *Proceedings of the national academy of sciences of the united states of america*, vol. 17, no. 5, pp. 315, 1931.
 - [52] Igor Mezić and Andrzej Banaszuk, “Comparison of systems with complex behavior,” *Physica D: Nonlinear Phenomena*, vol. 197, no. 1-2, pp. 101–133, 2004.
 - [53] Igor Mezić, “Spectral properties of dynamical systems, model reduction and decompositions,” *Nonlinear Dynamics*, vol. 41, no. 1, pp. 309–325, 2005.
 - [54] Marko Budišić and Igor Mezić, “Geometry of the ergodic quotient reveals coherent structures in flows,” *Physica D: Nonlinear Phenomena*, vol. 241, no. 15, pp. 1255–1269, 2012.
 - [55] Igor Mezić, “Analysis of fluid flows via spectral properties of the koopman operator,” *Annual Review of Fluid Mechanics*, vol. 45, pp. 357–378, 2013.
 - [56] Craig R Gin, Daniel E Shea, Steven L Brunton, and J Nathan Kutz, “Deepgreen: Deep learning of green’s functions for nonlinear boundary value problems,” *arXiv preprint arXiv:2101.07206*, 2020.
 - [57] Steve Plimpton, “Fast parallel algorithms for short-range molecular dynamics,” *Journal of computational physics*, vol. 117, no. 1, pp. 1–19, 1995.
 - [58] Hui Zhang, Zhongwu Liu, Xichun Zhong, Dongling Jiao, and Wanqi Qiu, “Lennard-jones interatomic potentials for the allotropes of carbon,” *arXiv preprint arXiv:1805.10614*, 2018.
 - [59] Minsu Cho, Jian Sun, Olivier Duchenne, and Jean Ponce, “Finding matches in a haystack: A max-pooling strategy for graph matching in the presence of outliers,” in *Proceedings of the IEEE Conference on Computer Vision and Pattern Recognition*, 2014, pp. 2083–2090.